# Luminescent Gold Nanocluster-Decorated Polymeric Hybrid Particles with Assembly-Induced Emission

Mathew Hembury,[†] Nataliia Beztsinna,[†] Hamed Asadi,[†] Joep B. van den Dikkenberg,[†] Johannes D. Meeldijk,[‡] Wim E. Hennink,[†] and Tina Vermonden*,[†]

[†]Department of Pharmaceutics, Utrecht Institute for Pharmaceutical Sciences (UIPS), Faculty of Science, Utrecht University, Universiteitsweg 99, 3584 CG Utrecht, The Netherlands

[‡]Electron Microscopy Group, Utrecht University, Padualaan 8, 3584 CH Utrecht, The Netherlands

S *Supporting Information*
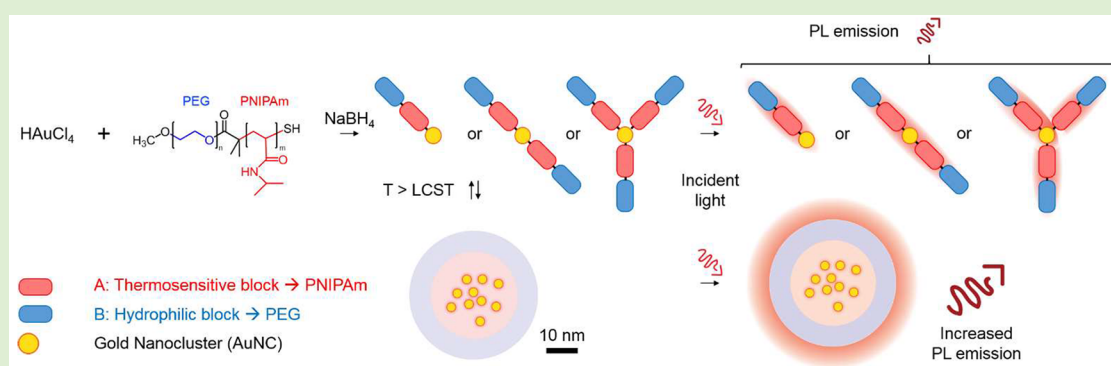
ABSTRACT: Ultrasmall gold atom clusters (<2 nm in diameter) or gold nanoclusters exhibit emergent photonic properties (near-infrared absorption and emission) compared to larger plasmonic gold particles because of the significant quantization of their conduction band. Although single gold nanocluster properties and applications are being increasingly investigated, little is still known about their behavior and properties when assembled into suprastructures, and even fewer studies are investigating their use for biomedical applications. Here, a simple synthetic pathway combines gold nanoclusters with thermosensitive diblock copolymers of poly(ethylene glycol) (PEG) and poly(N-isopropylacrylamide) (PNIPAm) to form a new class of gold-polymer, micelle-forming, hybrid nanoparticle. The nanohybrids' design is uniquely centered on enabling the temperature-dependent self-assembly of gold nanoclusters into the hydrophobic cores of micelles. This nonbulk assembly not only preserves but also enhances the attractive near-infrared photonics of the gold nanoclusters by significantly increasing their native fluorescent signal. In parallel to the fundamental insights into gold nanocluster ordering and assembly, the gold-polymer nanohybrids also demonstrated great potential as fluorescent live-imaging probes in vitro. This innovative material design based on the temperature-dependent, self-assembly of gold nanoclusters within a polymeric micelle's core shows great promise toward bioassays, nanosensors, and nanomedicine.

INTRODUCTION

With the emergence of nanoscience and nanotechnology, gold is increasingly becoming a key material for use in nanoparticle (NP) systems due to a variety of highly attractive properties.[1−3] In particular, light can collectively excite the free electrons of the metal to give rise to plasmonic responses in sub-100 nm gold NPs (AuNPs). This surface plasmon resonance (SPR) is the basis of many bioassays as its resonance peak is highly dependent on the size, shape, and aggregation state of the AuNPs. When reducing the size of the gold particles even further to the atomic scale (<2 nm, ∼300 atoms), a new set of unique molecule-like properties appears due to the significant quantization of the conduction band.[4,5] These quantum-sized AuNPs have discrete electronic energy levels as opposed to the continuous band in larger plasmonic AuNPs.[6] Ultrasmall gold atom clusters or gold nanoclusters (AuNCs) show multiple

optical absorption peaks in the optical spectrum compared to a single SPR peak between 500 and 600 nm for larger AuNPs.[5,7] The loss of the SPR and the appearance of fluorescent or even magnetic properties make these quantum-sized AuNPs a new class of nanomaterial, which explains the increasing interest toward them in recent years from the scientific community.[8,9]

This increased interest goes hand in hand with major advances in the synthesis and characterization of atomically precise AuNCs[7] as well as the development of theoretical models of their emergent properties and behavior.[5] Currently, high-yield, one-pot synthesis of atomically precise AuNCs has been achieved enabling the proliferation of studies centered on

AuNCs.[10−12] From mostly theoretical analyses, AuNCs have already shown promise for catalysis,[13] chemical sensing,[8] electronics,[14] and bioapplications including bioassays,[8,15] biological labeling,[8] and nanomedicine.[4,8] In particular, AuNCs absorb light in the near-infrared (NIR) biological window (650−900 nm)[16] and convert it to photons and heat, making AuNCs an excellent candidate for photoinduced cancer imaging and therapy.[4] In particular, AuNCs stabilized in the pores of mesoporous silica shells have been used in vivo as efficient multimodal imaging and therapy agents, demonstrating tumor burden reduction as well as enabling three complementary imaging modalities (fluorescent, photoacoustic, and magnetic resonance imaging).[4] Unfortunately, the clear therapeutic and imaging potential of AuNCs in vivo has been undermined so far by their lack of stability in biological environments.[4] Moreover, poor understanding of the aggregation behavior of AuNCs has hindered their potential for nanotechnology-based biomedical applications.

Polymeric micelles are one of the most established nanotechnology-based systems for anticancer therapy as they often show good biocompatibility, can be tailored through surface modifications, provide good pharmacokinetic control, and can easily trap and deliver anticancer drugs in particular hydrophobic drugs.[17−20] For example, micelles consisting of self-assembling diblock copolymers composed of a hydrophilic poly(ethylene glycol) (PEG) block and a thermosensitive N-isopropylacrylamide (NIPAm) block provide a useful yet simple platform for drug delivery and other biological applications.[21,22] The attractive cloud point temperature of PNIPAm at 32 °C allows for the self-assembly of the micelles at body temperature, and the PEG corona stabilizes and prevents the aggregation of the micelles in biological environments.[23,24] In this paper, we present a novel nanohybrid system consisting of AuNCs stabilized by thiol-terminated, thermosensitive diblock copolymers of PEG-PNIPAm, which reversibly self-assemble into micelles above their lower critical solution temperature (LCST). The resulting thermosensitive gold-polymer micelles were used to investigate the effect of AuNCs assembly into ordered structures or suprastructures.

Although the importance of the electronic environment around the AuNCs has been extensively described in the literature,[5,25] most studies so far investigated the effect of ligand composition or solvent and little is known about the effect of interparticle interactions between AuNCs upon assembly into suprastructures. By ordering NPs into arrays with recurring motifs (i.e., superlattices), structure-dependent properties arise from the newly formed suprastructures.[26,27] The nonadditivity of nanoscale interparticle interactions explains in part the large variation in NP suprastructure behavior observed and presents an intriguing puzzle to comprehend.[28] The versatility in superlattice composition and structure suggests that controlled NP self-assembly could turn out to be an important means toward the design of next-generation materials.[26,27,29,30] Here, we present evidence of the importance of interactions of AuNCs by investigating a novel, controllable, self-assembling gold-polymer nanohybrid platform, which itself shows promise toward fluorescent live-imaging applications.

■ MATERIALS AND METHODS

All materials were obtained from Sigma-Aldrich (Zwijndrecht, The Netherlands) and used as received unless indicated otherwise. Tetrahydrofuran (THF), N,N-dimethylformamide (DMF), and diethyl ether were purchased from Biosolve (Valkenswaard, The Nether-

lands). PBS buffer pH 7.4 (8.2 g/L NaCl, 3.1 g/L $Na_2HPO_4\cdot12H_2O$, 0.3 g/L $NaH_2PO_4\cdot2H_2O$) was purchased from B. Braun (Melsungen, Germany). Dulbecco's modified Eagle's medium (DMEM) and fetal bovine serum (FBS) were purchased from Sigma-Aldrich (Zwijndrecht, The Netherlands). Hoechst 33342 solution and phenol red free OptiMEM medium were purchased from Thermo Fisher Scientific (Bleiswijk, The Netherlands).

Synthesis of Gold-Polymer Nanohybrids. *Reversible Addition−Fragmentation Chain Transfer (RAFT) Polymerization of NIPAm.* In a typical experiment, N-isopropylacrylamide (NIPAm, 1.32 g, 11.6 mmol), poly(ethylene glycol) methyl ether 2-(dodecylthiocarbonothioylthio)-2-methylpropionate (PEG5000-CTA, 0.6 g, 0.12 mmol), 2,2′-azobis(2-methylpropionitrile) (AIBN, 3.94 g, 0.024 mmol) as the thermal initiator ([CTA]:[AIBN] = 5:1), and dry dimethylformamide (DMF, 300 mg of monomer per mL) were placed in a Schlenk flask, which was degassed by 3 freeze−pump−thaw cycles, backfilled with N_2, sealed, and heated under stirring to 70 °C. After 16 h, the reaction was quenched by placing the flask in an ice/water bath under air. The polymer was isolated by a 2-fold precipitation in cold diethyl ether and dried under vacuum, yielding a slightly yellow fine powder (yield of 61%). The conversion was calculated by ^{1}H NMR from the integrals of the characteristic poly(ethylene glycol) (PEG) and NIPAm peaks at 3.75 and 4.0 ppm, respectively, and was found to be 79%.

Aminolysis of the Trithiocarbonate Group (CTA) of the PEG-PNIPAm-CTA. The polymer (∼200 mg) was reacted with excess n-butylamine (30 equiv) in dry tetrahydrofuran (THF, 2 mL) for 3 h.[21] The color of the solution changed from light yellow to colorless. A few drops of n-tributylphosphine were added to the mixture to minimize disulfide formation.[21] The polymer was subsequently isolated by 2-fold precipitation in cold diethyl ether and obtained as a white solid after drying.

Gold-Polymer Nanohybrid Synthesis. The gold-polymer nanohybrids (PEG-PNIPAm-Au) were obtained by using the thiol-terminated PEG-PNIPAm-SH polymers as stabilizing ligands. In a typical reaction, gold(III) chloride trihydrate salt (2.4 mg) and PEG-PNIPAM-SH polymers (500 mg) were suspended in Milli-Q water (9.8 mL) and stirred at slow speed at room temperature for 1 h ([Au]:[SH] = 1:3). The color of the mixture changed from yellow to colorless. After increasing the stirring speed, sodium borohydride (0.69 mg, 0.2 mL) was added dropwise, and the reaction mixture was left to react overnight at room temperature. The next day, the mixture had a dark yellow/brown color. The gold-polymer nanohybrids were dialyzed (10 kDa MWCO) against water at 4 °C for 1 day before being freeze-dried.

Lipoic Acid-Stabilized Gold Nanocluster Synthesis. The control free lipoic acid-stabilized gold nanoclusters were synthesized using a slightly modified version of the gold-polymer nanohybrids. Instead, the thiol-terminated polymer was replaced by lipoic acid (3.77 mg) while keeping the 1:3 gold to thiol ratio. The reaction mixture was purified from free ligands by applying 3 cycles of centrifugation/filtration using a membrane filtration device with a molecular weight cutoff of 10 kDa (Millipore).

Characterization of Gold-Polymer Nanohybrids. *Nuclear Magnetic Resonance (NMR) Spectroscopy.* ^{1}H NMR (400 MHz) was measured on an Agilent 400-MR NMR spectrometer (Agilent Technologies, Santa Clara, USA). The chemical shifts were calibrated against residual solvent peaks of $CDCl_3$ (δ = 7.26 ppm).

Gel Permeation Chromatography (GPC). GPC was performed using a Plgel 5 μm mixed-D column (Polymer Laboratories) and a refractive index detector (RID). The eluent was DMF containing 10 mM LiCl; the elution rate was set to 1 mL min^{-1}, and the temperature was set to 65 °C. The sample concentration was 10 mg mL^{-1}. PEGs of narrow and defined molecular weights were used as calibration standards.

Dynamic Light Scattering (DLS). DLS measurements were performed on a Malvern CGS-3 goniometer coupled to an AVL/LSE-5003 autocorrelator, a thermostated water bath, and a He−Ne laser (25 mW, 633 nm, equipped with a model 2500 remote interface controller, Uniphase). All measurements were carried out at 90° angle

with temperatures ranging from 10 to 55 °C. The solvent viscosity was corrected for each temperature by the software. The z-average radius and polydispersity index were calculated by ALV and DTS software, respectively.

Cloud Point Determination. Cloud points were determined by measuring the onset of opalescence with light scattering. Light scattering intensity was measured using a Jasco FP-8300 spectrophotometer with both emission and excitation wavelength set at 550 nm with 1 nm slits and response time of 1 s. A temperature ramp of 1 °C per min from 15 to 55 °C was applied. For the thermal stability study, light scattering intensity at 600 nm was measured during 5 repeated temperature cycles (10 to 45 °C). Additionally, the transition temperature was measured for PEG-PNIPAm-Au samples by photoluminescence at 750 nm by the onset of increased intensity. The measurement setup is described below (Steady-State Photoluminescent Spectroscopy).

UV−Vis Spectroscopy. UV−vis measurements were collected using a 10 mm path-length quartz cuvette in a Shimadzu UV 2450 spectrophotometer from 250 to 400 nm with 0.5 nm resolution. Samples were dissolved in THF (1 mg mL^{-1}) after the aminolysis step of the thiol-terminated polymer.

Steady-State Photoluminescent Spectroscopy. Steady-state photoluminescence measurements were collected using a 10 mm path length quartz cuvette using a Jasco FP-8300 spectrophotometer with a response time of 1 s, 5 nm slits, and resolution of 0.5 nm. Emission spectra were collected from 560 to 900 nm with excitation at 550 nm. Excitation spectra were collected from 300 to 710 nm by acquiring the emission intensity at 720 nm. Samples were dispersed in Milli-Q water, PBS, or phenol red free OptiMEM media (1 mg mL^{-1}), and the samples were scanned at 10 °C unless otherwise stated. For the determination of the temperature-dependent profile, a temperature ramp of 1 °C per min from 10 to 60 °C was used. For the thermal stability study, fixed-wavelength measurements were used collecting the fluorescent emission intensity at 720 nm when excited at 550 nm during 5 repeated temperature cycles (10 to 45 °C).

Quantum Yield Calculation. The quantum yields (QYs) were calculated relative to Qdot 800 ITK Carboxyl Quantum Dots (Invitrogen; $QY = 0.62$) in Milli-Q water. The extinction E of both the reference Qdot and samples were adjusted to be below 0.2 optical density at the excitation wavelength to minimize luminescence quenching due to internal reabsorption. The final QYs of the samples were calculated according to

$$QY = QY_{ref} \frac{I}{I_{ref}} \frac{n^2}{n_{ref}^2} \frac{(1 - 10^{-E})^{ref}}{1 - 10^{-E}}$$

where n is the refractive index, I is the integrated luminescence intensity, and ref denotes the reference sample (Qdot 800 ITK Carboxyl Quantum Dots).[31]

Electron Microscopy. Transmission electron microscopy (TEM) was used to determine the morphology of the gold-polymer nanohybrids. Bright field TEM and high angle annular dark field scanning TEM (HAADF-STEM) images of the particles were acquired using a Tecnai20F (FEI) microscope equipped with a Gatan CCD camera (model 694) and an energy-dispersive X-ray spectroscopy (EDS) detector (Oxford Instrument) operated at an accelerating voltage of 200 kV. Samples were dissolved in Milli-Q water (1 mg mL^{-1}). The samples were then left at the desired temperature (10 or 45 °C) for 30 min before being drop-deposited on 200 mesh carbon-coated copper TEM grids (Agar Scientific) prior to analysis.

EDS analysis was used to quantify the chemical composition of the gold-polymer nanohybrids. X-ray counts were recorded during a 1 min period at 10 kV and analyzed using INCA Energy 3000 software (Oxford Instruments).

Cytotoxicity and Internalization Studies. *Cell Culture.* The human liver carcinoma HepG2 cells used in this study were obtained from American Type Culture Collection (ATCC). The cells were maintained in an incubator at a temperature of 37 °C, regulated with 5% CO$_2$, 95% air, and saturated humidity. Dulbecco's modified Eagle's medium (DMEM) supplemented with 10% (v/v) fetal bovine serum

(FBS, Sigma) was used as the cell culture medium. The cell medium was changed every 2−4 days, and the cells were passed using trypsin-ethylenediaminetetraacetic acid (trypsin-EDTA) upon reaching 80% confluency.

MTS Assay. HepG2 cells were cultured in 96-well plates (Greiner). Briefly, the cells were seeded at a density of 1×10^4 cells cm^{-2} and after 16 h were cultured with gold polymer nanohybrids or lipoic acid-stabilized AuNCs at concentrations ranging from 0.05 to 10 mg mL^{-1}. Samples of 500 μM SDS were used as negative control. The cells were incubated in a cell culture incubator at 37 °C with 5% CO$_2$ for 24 h. Afterward, the media containing the particles was removed and replaced with 100 μL of growth medium and 20 μL of 5-(3-carboxymethoxyphenyl)-2-(4,5-dimenthylthiazoly)-3-(4-sulfophenyl)-tetrazolium salt (MTS) solution (CellTiter 96 Aqueous one Cell proliferation Assay, Promega). After 1 h incubation time at 37 °C, the absorbance was monitored using a microplate reader (Spectrostar) at a wavelength of 490 nm with a reference wavelength at 650 nm. The cytotoxicity was expressed as the percentage of cell viability compared with untreated cell controls. The experiment was run in triplicate, and the results are presented as percent averages ± standard deviations. The negative control, 500 μM sodium dodecyl sulfate (SDS), was added to the medium on cells and left in the incubator for 24 h. The sample is used in the same way as the particle-containing sample media.

Laser Confocal Scanning Microscopy. HepG2 cells were cultured in 6-chamber Ibidi slides (Ibidi, Germany). Briefly, the cells were seeded at a density of 10^4 cells cm^{-2} and cultured for 1 day with gold-polymer nanohybrids (10 mg mL^{-1}) or lipoic acid-stabilized AuNCs (0.5 mg mL^{-1}). After the medium was removed, the cells were washed 3 times with phosphate buffered saline (PBS, pH 7.4) and fixed with 4% (v/v) paraformaldehyde (PFA) in PBS. Hoechst 33342 stain was used to stain the cell nuclei. The Hoechst solution was added under dark conditions for 10 min at 37 °C. Between each step, the samples were washed twice with PBS. The plates were visualized under a confocal microscope (Leica TCS SP8 X MP), and the images were analyzed with LAS X (Leica Microsystems).

■ RESULTS AND DISCUSSION

We synthesized gold-polymer nanohybrids composed of gold nanoclusters (AuNCs) stabilized with thermosensitive diblock copolymers of poly(ethylene glycol) (PEG) and poly(N-isopropylacrylamide) (PNIPAm). First, a thiol-terminated PEG-PNIPAm was obtained by a two-step synthesis. Reversible addition−fragmentation chain transfer (RAFT) polymerization was used to add NIPAm to the commercially available PEGylated RAFT chain transfer agent poly(ethylene glycol) methyl ether 2-(dodecylthiocarbonothioylthio)-2-methylpropionate (Scheme S1 (1)) to obtain the desired thermosensitive diblock copolymer. RAFT polymerization was chosen as it allows the retention of a trithiocarbonate functional group present on the chain transfer agent (CTA) at the end of the polymerization process, which was subsequently converted to a thiol functional group.[21,32] The successful polymerization of NIPAm to the PEG-CTA was confirmed using gel permeation chromatography (GPC) and ^{1}H nuclear magnetic resonance (NMR) spectroscopy. The results showed that the experimental number-average molecular weight (∼14 kDa) of the diblock copolymer was in good agreement with the expected molecular weight based on the feed ratio of initiator to NIPAm monomers ([initiator]:[monomer] = 1:500) and the target conversion rate of 70−80% (Table S1). This conversion was also confirmed by ^{1}H NMR (Figure S1), and the maximum conversion of 80% was chosen to avoid the loss of the end groups due to radical side reactions at high conversion.[21] The dispersity was relatively narrow (≤1.2) as can be expected for this type of polymerization reaction.[33]
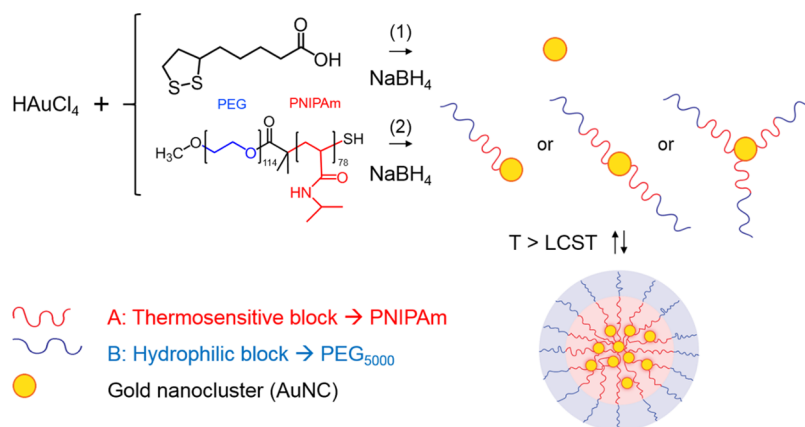
Figure 1. Schematic of gold nanocluster (AuNC) synthesis using (1) lipoic acid as stabilizing agent and (2) thiol-terminated, thermosensitive PEG-PNIPAm-SH polymers as ligands and micelle formation upon heating above their lower critical solution temperature (LCST). The resulting micelles are composed of a protective PEG shell (blue) and a thermosensitive inner core of NIPAm (red) and AuNCs (yellow).
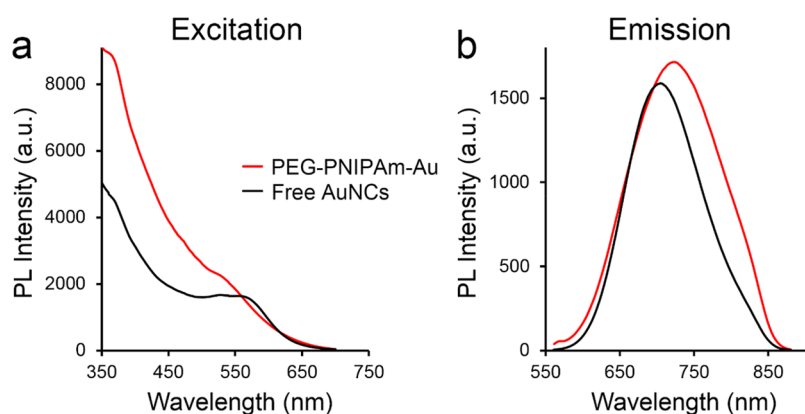

Figure 2. Gold-polymer nanohybrid optical properties: near-infrared photoluminescence. Photoluminescent (a) excitation (λ_{em} = 720 nm) and (b) emission (λ_{ex} = 550 nm) spectra at 10 °C of lipoic acid-stabilized AuNCs (free AuNCs, black) and gold-polymer nanohybrids (PEG-PNIPAm-Au, red) showing emission peaks centered at 703 and 720 nm, respectively.

The second step consisted of converting the trithiocarbonate group at the ω-chain end of the PEG-PNIPAm-CTA to a thiol by aminolysis (Scheme S1 (2)).[21] The conversion of this reaction was followed via UV−vis spectroscopy, as the trithiocarbonate group has a characteristic absorbance at 310 nm where the thiol group does not absorb.[34] After 3 h, complete disappearance of the signal at 310 nm was observed, reflecting the full conversion of the trithiocarbonate (Figure S2). Furthermore, no significant shift in the molecular weight distribution was observed in the GPC chromatograms, confirming the absence of disulfide bridge formation between two PEG-PNIPAm-SH polymers.

Finally, gold-polymer nanohybrids were prepared by nucleating gold in the presence of the synthesized thiol-terminated, thermosensitive polymeric ligands. Briefly, an excess of thiolated PEG-PNIPAm-SH was added to a gold(III) chloride trihydrate ($HAuCl_4$) solution to form gold(I)-thiol complexes before the final reduction to gold(0) using sodium borohydride ($NaBH_4$) (Figure 1). Gold-polymer nanohybrids were formed, resulting in particles with likely a varying number of thiolated polymeric ligands. In parallel, control AuNCs that do not exhibit temperature-dependent self-assembly were synthesized using a similar synthetic method but using lipoic acid as stabilizing agent[35] rather than the thiol-terminated, thermosensitive polymers.

The thermosensitive properties of the thiol-terminated PEG-PNIPAm-SH were investigated by light scattering, and the polymer showed a cloud point temperature of 34.8 ± 0.4 °C and micelles of 42 nm in diameter with a narrow size distribution (PDI 0.06, dynamic light scattering analysis) above their cloud point (Table S2). Upon conjugation of AuNCs to the polymer, the cloud point shifted to 36.6 ± 2.5 °C, and the diameter of the micelles decreased to 37 nm (PDI 0.10, dynamic light scattering analysis) (Table S2). Remarkably, the transition temperature found with photoluminescence at 750 nm showed a slightly lower value of 30.2 ± 1.5 °C, indicating that self-assembly occurred even before significant scattering of the samples became visible. The slight shift in the cloud point to higher temperature upon attachment of the AuNCs indicated that the PNIPAm block becomes less prone to dehydration and that apparently the AuNCs contributed to an overall increase in hydrophilicity. Adding a thermosensitive block to the polymeric ligands not only enables an easy and reversible formation of the AuNC-containing micelles but also enables the gold-polymer nanohybrids to exhibit enhanced fluorescent emission at body temperature.

Below their cloud point temperature, the gold-polymer nanohybrids displayed a distinct near-infrared (NIR) fluorescent profile as expected for the photonics properties of AuNCs in general (Figure 2). However, compared to the lipoic acid-stabilized AuNCs, the gold-polymer nanohybrids displayed a
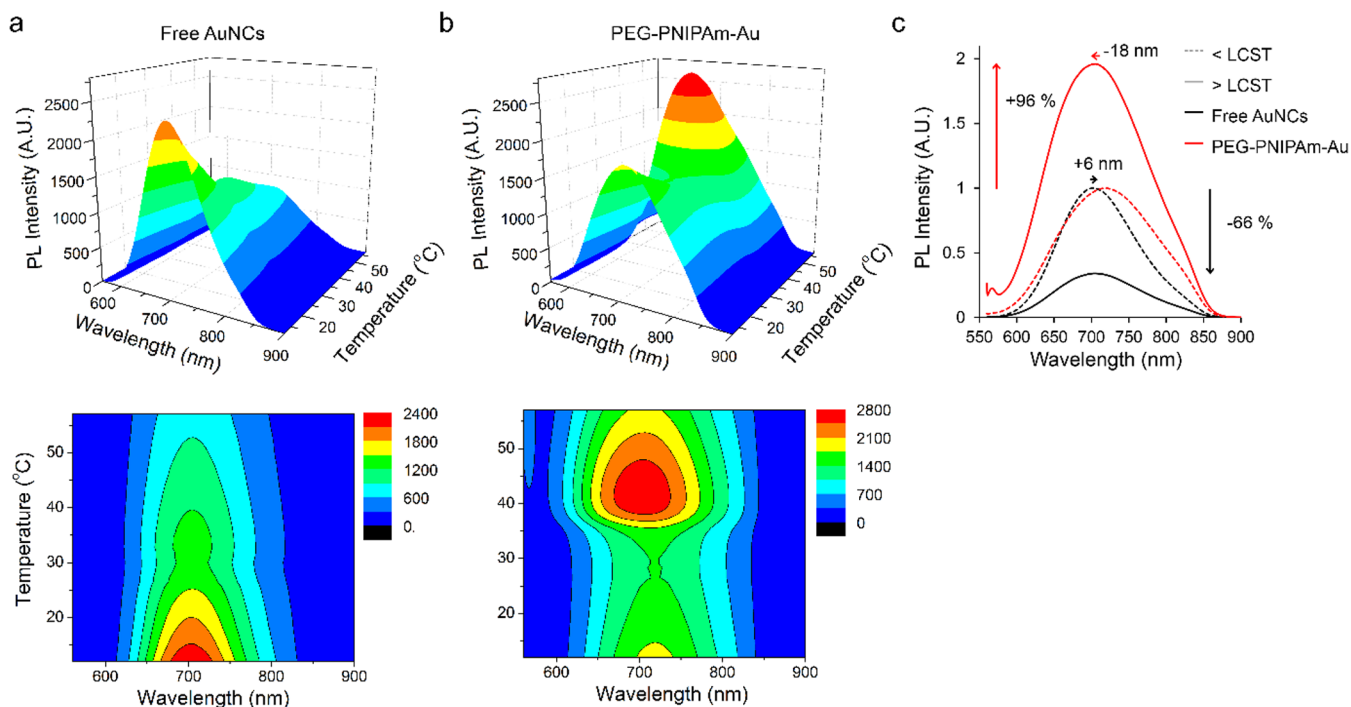
Figure 3. Temperature-dependent photoluminescent properties. (a, b) Temperature-dependent 3D fluorescent profile and corresponding heatmaps of (a) lipoic acid-stabilized AuNCs (free AuNCs) and (b) gold-polymer nanohybrids (PEG-PNIPAm-Au) showing an increase and blue-shift of the photoluminescent peak above the lower critical temperature (LCST) of the gold-polymer nanohybrids indicating an effect of the assembly of the AuNCs in the core of the micelles. (c) Emission spectra under (dotted line) and over (plain line) the LCST normalized to the maximum peak intensity under the LCST of lipoic acid-stabilized AuNCs (black) and PEG-PNIPAm-Au (red) (λ_{ex} = 550 nm).

fluorescent emission mode at 720 nm compared to 703 nm for lipoic acid-stabilized AuNCs and an increased quantum yield of 3.6% compared to 2.7%. The gold-polymer nanohybrid quantum yield is significantly higher than most other AuNC-based systems reported in the literature (<1%).[7,8,36] In addition, although the lipoic acid-stabilized AuNCs exhibited a broad excitation shoulder centered around 550 nm, the excitation profile was practically featureless for the gold-polymer nano-hybrids.

Furthermore, the gold-polymer nanohybrids exhibited not only fluorescent properties in the NIR biowindow but also a nonmonotonic, temperature-dependent fluorescent profile (Figure 3). Compared to the typical decrease in fluorescence intensity with increasing temperature observed for the lipoic acid-stabilized AuNCs, the gold-polymer nanohybrids displayed first a decrease in fluorescence until 29 °C before the fluorescence sharply increased until 42 °C to finally resume into a linear decrease with increasing temperature. When heated above their cloud point, the gold-polymer nanohybrids formed micelles, and the AuNCs self-assemble within the micelles' hydrophobic cores. The morphology of lipoic acid-stabilized AuNCs and the gold-polymer nanohybrids was investigated by transmission electron microscopy (TEM) and showed spherical particles (∼1.5 nm) for the lipoic acid-stabilized AuNCs (Figure S3) and larger spherical particles (∼50 nm) for the gold-polymer nanohybrids at temperatures over the LCST with focal points of higher contrast (<2 nm) observed within the core of the nanohybrids (Figure 4). High-angle annular dark field scanning TEM (HAADF-STEM) was used to complement the bright field TEM study, highlighting all gold nanostructures present in the gold-polymer nano-hybrids both below and above the LCST (Figure 4). Finally, energy-dispersive X-ray spectroscopy (EDS) (Figure S4)
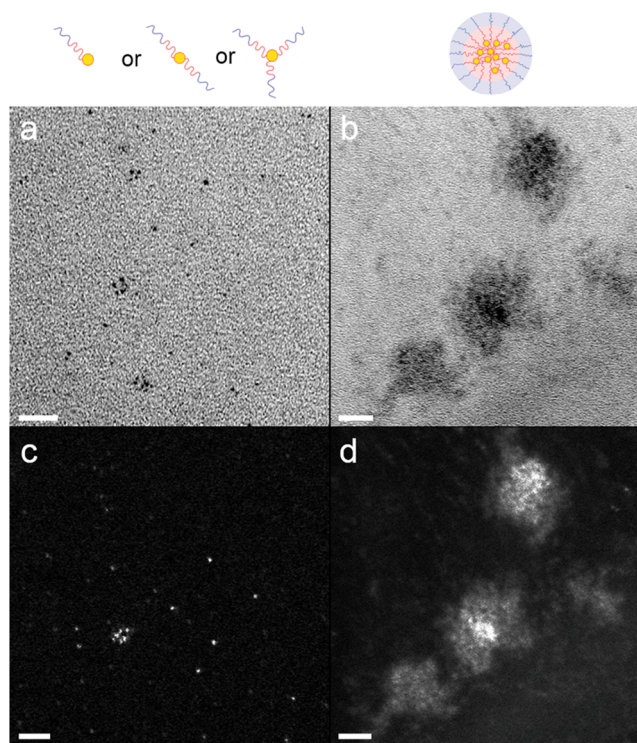

Figure 4. Gold-polymer nanohybrid morphology. (a, b) Bright field transmission electron microscopy (TEM) images of gold-polymer nanohybrids (b) below and (c) over the LCST. (c, d) High-angle annular dark field scanning transmission electron microscopy (HAADF-STEM) images of gold-polymer nanohybrids highlighting the gold nanostructures within the nanohybrids (c) below and (d) over the LCST. Scale bars: 20 nm.
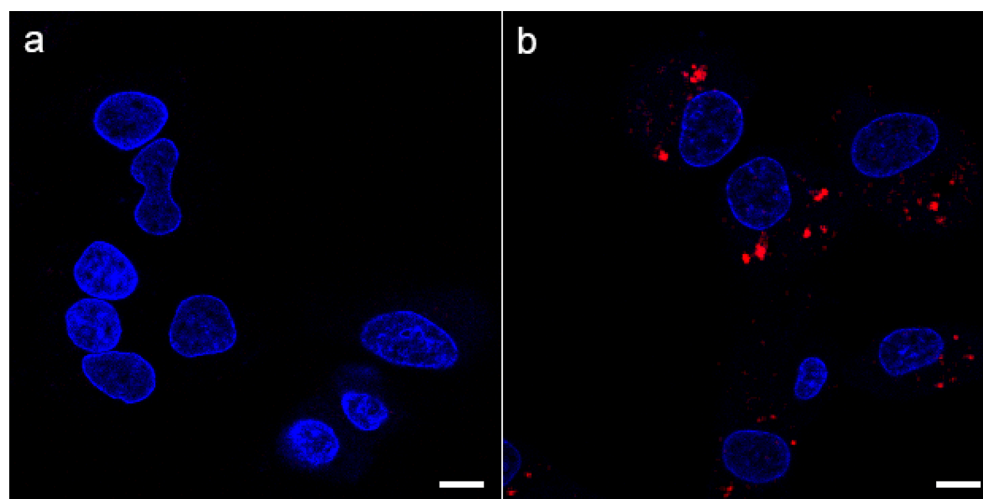
Figure 5. Laser confocal scanning microscopy images of HepG2 cells incubated for 24 h at 37 °C with (a) cell culture media and (b) gold-polymer nanohybrids. Cells are stained for nucleus (Hoechst, blue). The gold-polymer nanohybrids are localized by their native fluorescence (red) within the cells. Scale bars: 10 μm.

confirmed the presence of gold within the gold-polymer nanohybrids.

Upon heating, the free lipoic acid-stabilized AuNC control showed a linear decrease in fluorescent intensity with a 66% maximum decrease and a maximum red-shift of 6 nm in its fluorescent profile between the lowest and highest temperatures investigated (Figure 3c, Table S2). This decrease in fluorescence intensity is expected due to the higher amount of the incident energy being lost to nonradiative pathways as the temperature increases. In comparison, the temperature-dependent self assembly of the gold-polymer nanohybrids induced a maximum blue-shift of 18 nm in the fluorescent emission peak and a 96% increase in the fluorescent signal intensity (Figure 3c, Table S2). This significant emission enhancement can be attributed to the energy transfer between AuNCs due to the reduced intercluster distance within the polymeric micelles' hydrophobic cores.[37,38] Even without an ordered assembly (i.e., constant spacing of AuNCs), the AuNCs interacted constructively with regards to their fluorescence when their spacing is reduced, thereby overcoming and even enhancing the natural decrease in fluorescent intensity upon heating. The temperature driven, nonmonotonic fluorescent emission profile of the gold-polymer nanohybrids starting at 29 °C demonstrates that interparticle interactions between AuNCs is a key component to achieve a comprehensive understanding of AuNC behavior.

By using thermosensitive polymers as capping ligands for AuNCs, the stability issue in aqueous media of the AuNCs is circumvented while preserving and enhancing the AuNCs NIR absorption and emission. In particular, whereas the fluorescent intensity of the lipoic acid-stabilized AuNCs decreased with time (40% in 2 months in water at room temperature, Figure S5), indicating coalescence of the AuNCs, the gold-polymer nanohybrids fluorescent profile remained stable during the same period of time at room temperature demonstrating that the polymeric ligands act as a protective, stabilizing framework that allow the AuNCs to retain their advantageous properties in aqueous solution. In addition, gold-polymer nanohybrids dispersed in PBS or media did not exhibit any decrease in fluorescence, further confirming their stability in more complex media. Repeated temperature cycles from 10 to 45 °C (below

and above the LCST, respectively) did not affect the size, PDI, or fluorescent emission of the gold-polymer nanohybrids demonstrating the thermal stability of the system (Figure S6). Furthermore, the high photothermal conversion of AuNCs[4] could potentially enable photoinduced rather than temperature-driven assembly of the micelles.

As a first step toward assessing the gold-polymer nanohybrid potential for bioapplications, in vitro testing demonstrated that the gold-polymer nanohybrids did not exhibit cytotoxicity over 1 day in HepG2 cells at 37 °C at all concentrations tested (up to 10 mg mL^{-1}) (Figure S7). On the other hand, lipoic acid-stabilized AuNCs significantly decreased cell viability at concentrations as low as 0.25 mg mL^{-1}. Furthermore, the gold-polymer nanohybrids were internalized after 24 h in HepG2 cells at 37 °C, whereas lipoic acid-stabilized AuNCs aggregated outside the cells and were toxic (Figure S8). Although 37 °C is below the gold-nanohybrids' LCST, the nanohybrids still exhibited enhanced fluorescence at body temperature with a 61% increased fluorescent signal intensity compared to the fluorescence intensity at 29 °C. Importantly, the gold-polymer nanohybrid conjugates were localized using their native fluorescence, demonstrating their potential as fluorescent live-imaging contrast agents (Figure 5). The fluorescent images showed gold-polymer nanohybrid conjugates localized within vesicular structures inside the cells' cytoplasm and accumulating in the perinuclear region (Figure 5). This is compatible with endocytotic processes that internalize particles and traffic them through the endolysosomal system to finally accumulate in vesicles within the cells.[39]

■ CONCLUSIONS

With the use of AuNCs for biomedical applications in its infancy, this study points out the importance of the AuNCs direct electronic environment. The gold-polymer nanohybrid system described here demonstrates that the design of smart ligands that can control the immediate environment of the AuNCs can not only help the stabilization of AuNCs in biological environments but also give rise to new patterns in the unique properties of the AuNCs. By using thermosensitive polymers as ligands for AuNCs, we studied the effect of controlled, temperature-driven aggregation of AuNCs on their

native fluorescence. The results demonstrated that the nonbulk assembly of AuNCs into the core of polymeric micelles significantly increased their native fluorescent signal. In parallel to the fundamental insights into AuNC ordering and assembly, the gold-polymer nanohybrids demonstrate their great potential as fluorescent live-imaging probes in vitro. Moreover, the gold-polymer nanohybrids have been shown to exhibit not only properties from both the gold and polymer components (fluorescence- and temperature-triggered self assembly, respectively) but also properties that arise from the two components synergistic interaction. In a broader context, the gold-polymer nanohybrids ability to stabilize a large number of AuNCs and enhance their fluorescence indicates their potential for applications in cancer treatment, catalysis, nanosensing as well as label-free chemical and biochemical detection.

■ ASSOCIATED CONTENT

ⓢ Supporting Information

The Supporting Information is available free of charge on the ACS Publications website at DOI: 10.1021/acs.biomac.8b00414.

> Synthetic scheme for thiol-terminated thermosensitive polymer (SI-Scheme 1); ^{1}H NMR spectra of thermosensitive polymers (SI-Figure 1); UV−vis spectra of polymers before and after aminolysis (SI-Figure 2); TEM image of free lipoic acid-stabilized AuNCs (SI-Figure 3); elemental analysis of gold-polymer nanohybrids (SI-Figure 4); photostability of gold-polymer nanohybrids (SI-Figure 5); thermal stability of gold-polymer nanohybrids and lipoic acid-stabilized AuNCs (SI-Figure 6); MTS cytocompatibility (SI-Figure 7); laser confocal scanning microscopy image of HepG2 cells incubated with lipoic acid-stabilized AuNCs (SI-Figure 8); properties of PEG-PNIPAm polymers (Table S1); and summary of nanoparticle properties (Table S2) (PDF)

■ AUTHOR INFORMATION

Corresponding Author

*E-mail: t.vermonden@uu.nl; phone: +31 (0)30 253 7306.

ORCID ⓘ

Mathew Hembury: 0000-0002-7949-0027
Wim E. Hennink: 0000-0002-5750-714X
Tina Vermonden: 0000-0002-6047-5900

Notes

The authors declare no competing financial interest.

■ ACKNOWLEDGMENTS

■ REFERENCES

(1) Daniel, M.; Astruc, D. Gold Nanoparticles: Assembly, Supramolecular Chemistry, Quantum-Size-Related Properties, and Applications Toward Biology, Catalysis, and Nanotechnology. *Chem. Rev.* **2004**, *104*, 293−346.

(2) Llevot, A.; Astruc, D. Applications of Vectorized Gold Nanoparticles to the Diagnosis and Therapy of Cancer. *Chem. Soc. Rev.* **2012**, *41*, 242−257.

(3) Boisselier, E.; Astruc, D. Gold Nanoparticles in Nanomedicine: Preparations, Imaging, Diagnostics, Therapies and Toxicity. *Chem. Soc. Rev.* **2009**, *38*, 1759−1782.

(4) Hembury, M.; Chiappini, C.; Bertazzo, S.; Kalber, T. L.; Drisko, G. L.; Ogunlade, O.; Walker-Samuel, S.; Krishna, K. S.; Jumeaux, C.; Beard, P.; et al. Gold-Silica Quantum Rattles for Multimodal Imaging and Therapy. *Proc. Natl. Acad. Sci. U. S. A.* **2015**, *112*, 1959−1964.

(5) Qian, H.; Zhu, M.; Wu, Z.; Jin, R. Quantum Sized Gold Nanoclusters with Atomic Precision. *Acc. Chem. Res.* **2012**, *45*, 1470−1479.

(6) Kelly, K. L.; Coronado, E.; Zhao, L. L.; Schatz, G. C. The Optical Properties of Metal Nanoparticles: the Influence of Size, Shape, and Dielectric Environment. *J. Phys. Chem. B* **2003**, *107*, 668−677.

(7) Jin, R. Atomically Precise Metal Nanoclusters: Stable Sizes and Optical Properties. *Nanoscale* **2015**, *7*, 1549−1565.

(8) Jin, R.; Zeng, C.; Zhou, M.; Chen, Y. Atomically Precise Colloidal Metal Nanoclusters and Nanoparticles: Fundamentals and Opportunities. *Chem. Rev.* **2016**, *116*, 10346−10413.

(9) Pelaz, B.; Alexiou, C.; Alvarez-Puebla, R. A.; Alves, F.; Andrews, A. M.; Ashraf, S.; Balogh, L. P.; Ballerini, L.; Bestetti, A.; Brendel, C.; et al. Diverse Applications of Nanomedicine. *ACS Nano* **2017**, *11*, 2313−2381.

(10) Qian, H.; Zhu, Y.; Jin, R. Size-Focusing Synthesis, Optical and Electrochemical Properties of Monodisperse Au 38(SC 2H 4Ph) 24Nanoclusters. *ACS Nano* **2009**, *3*, 3795−3803.

(11) Yuan, X.; Zhang, B.; Luo, Z.; Yao, Q.; Leong, D. T.; Yan, N.; Xie, J. Balancing the Rate of Cluster Growth and Etching for Gram-Scale Synthesis of Thiolate-Protected Au 25Nanoclusters with Atomic Precision. *Angew. Chem., Int. Ed.* **2014**, *53*, 4623−4627.

(12) Zhu, M.; Qian, H.; Jin, R. Thiolate-Protected Au 24(SC 2H 4Ph) 20Nanoclusters: Superatoms or Not? *J. Phys. Chem. Lett.* **2010**, *1*, 1003−1007.

(13) Li, G.; Jin, R. Atomically Precise Gold Nanoclusters as New Model Catalysts. *Acc. Chem. Res.* **2013**, *46*, 1749−1758.

(14) Koh, T. W.; Hiszpanski, A. M.; Sezen, M.; Naim, A.; Galfsky, T.; Trivedi, A.; Loo, Y. L.; Menon, V.; Rand, B. P. Metal Nanocluster Light-Emitting Devices with Suppressed Parasitic Emission and Improved Efficiency: Exploring the Impact of Photophysical Properties. *Nanoscale* **2015**, *7*, 9140−9146.

(15) Shang, L.; Nienhaus, G. U. Small Fluorescent Nanoparticles at the Nano−Bio Interface. *Mater. Today* **2013**, *16*, 58−66.

(16) Jain, P. K.; Huang, X.; El-Sayed, I. H.; El-Sayed, M. A. Noble Metals on the Nanoscale: Optical and Photothermal Properties and Some Applications in Imaging, Sensing, Biology, and Medicine. *Acc. Chem. Res.* **2008**, *41*, 1578−1586.

(17) Deng, C.; Jiang, Y.; Cheng, R.; Meng, F.; Zhong, Z. Biodegradable Polymeric Micelles for Targeted and Controlled Anticancer Drug Delivery: Promises, Progress and Prospects. *Nano Today* **2012**, *7*, 467−480.

(18) Eetezadi, S.; Ekdawi, S. N.; Allen, C. The Challenges Facing Block Copolymer Micelles for Cancer Therapy: in Vivo Barriers and Clinical Translation. *Adv. Drug Delivery Rev.* **2015**, *91*, 7−22.

(19) Bertrand, N.; Leroux, J.-C. The Journey of a Drug-Carrier in the Body: an Anatomo-Physiological Perspective. *J. Controlled Release* **2012**, *161*, 152−163.

(20) Cabral, H.; Kataoka, K. Progress of Drug-Loaded Polymeric Micelles Into Clinical Studies. *J. Controlled Release* **2014**, *190*, 465−476.

(21) Wallyn, S.; Zhang, Z.; Driessen, F.; Pietrasik, J.; De Geest, B. G.; Hoogenboom, R.; Du Prez, F. E. E. Straightforward RAFT Procedure for the Synthesis of Heterotelechelic Poly(Acrylamide)S. *Macromol. Rapid Commun.* **2014**, *35*, 405−411.

(22) Topp, M. D. C.; Dijkstra, P. J.; Talsma, H.; Feijen, J. Thermosensitive Micelle-Forming Block Copolymers of Poly-(Ethylene Glycol) and Poly(N-Isopropylacrylamide). *Macromolecules* **1997**, *30*, 8518−8520.

(23) de Graaf, A. J.; Azevedo Próspero dos Santos, I. I.; Pieters, E. H. E.; Rijkers, D. T. S.; van Nostrum, C. F.; Vermonden, T.; Kok, R. J.; Hennink, W. E.; Mastrobattista, E. A Micelle-Shedding Thermosensitive Hydrogel as Sustained Release Formulation. *J. Controlled Release* **2012**, *162*, 582−590.

(24) de Graaf, A. J.; Boere, K. W. M.; Kemmink, J.; Fokkink, R. G.; van Nostrum, C. F.; Rijkers, D. T. S.; van der Gucht, J.; Wienk, H.; Baldus, M.; Mastrobattista, E.; et al. Looped Structure of Flowerlike Micelles Revealed by 1H NMR Relaxometry and Light Scattering. *Langmuir* **2011**, *27*, 9843−9848.

(25) Niihori, Y.; Kikuchi, Y.; Kato, A.; Matsuzaki, M.; Negishi, Y. Understanding Ligand-Exchange Reactions on Thiolate-Protected Gold Clusters by Probing Isomer Distributions Using Reversed-Phase High-Performance Liquid Chromatography. *ACS Nano* **2015**, *9*, 9347−9356.

(26) Boles, M. A.; Engel, M.; Talapin, D. V. Self-Assembly of Colloidal Nanocrystals: From Intricate Structures to Functional Materials. *Chem. Rev.* **2016**, *116*, 11220−11289.

(27) Ho-Wu, R.; Yau, S. H.; Goodson, T., III Linear and Nonlinear Optical Properties of Monolayer-Protected Gold Nanocluster Films. *ACS Nano* **2016**, *10*, 562−572.

(28) Silvera Batista, C. A.; Larson, R. G.; Kotov, N. A. Nonadditivity of Nanoparticle Interactions. *Science* **2015**, *350*, 1242477−12424770.

(29) Ye, X.; Zhu, C.; Ercius, P.; Raja, S. N.; He, B.; Jones, M. R.; Hauwiller, M. R.; Liu, Y.; Xu, T.; Alivisatos, A. P. Structural Diversity in Binary Superlattices Self-Assembled From Polymer-Grafted Nanocrystals. *Nat. Commun.* **2015**, *6*, 933.

(30) Zhang, Y.; Lu, F.; Yager, K. G.; van der Lelie, D.; Gang, O. A General Strategy for the DNA-Mediated Self-Assembly of Functional Nanoparticles Into Heterogeneous Systems. *Nat. Nanotechnol.* **2013**, *8*, 865−872.

(31) Grabolle, M.; Spieles, M.; Lesnyak, V.; Gaponik, N.; Eychmüller, A.; Resch-Genger, U. Determination of the Fluorescence Quantum Yield of Quantum Dots: Suitable Procedures and Achievable Uncertainties. *Anal. Chem.* **2009**, *81*, 6285−6294.

(32) Selvan, T.; Spatz, J. P.; Klok, H. A.; Möller, M. Gold−Polypyrrole Core−Shell Particles in Diblock Copolymer Micelles. *Adv. Mater.* **1998**, *10*, 132−134.

(33) Averick, S.; Mehl, R. A.; Das, S. R.; Matyjaszewski, K. Well-Defined Biohybrids Using Reversible-Deactivation Radical Polymerization Procedures. *J. Controlled Release* **2015**, *205*, 45−57.

(34) Skrabania, K.; Miasnikova, A.; Bivigou-Koumba, A. M.; Zehm, D.; Laschewsky, A. Examining the UV-Vis Absorption of RAFT Chain Transfer Agents and Their Use for Polymer Analysis. *Polym. Chem.* **2011**, *2*, 2074−2083.

(35) Aldeek, F.; Muhammed, M. A. H.; Palui, G.; Zhan, N.; Mattoussi, H. Growth of Highly Fluorescent Polyethylene Glycol- and Zwitterion-Functionalized Gold Nanoclusters. *ACS Nano* **2013**, *7*, 2509−2521.

(36) Goswami, N.; Yao, Q.; Luo, Z.; Li, J.; Chen, T.; Xie, J. Luminescent Metal Nanoclusters with Aggregation-Induced Emission. *J. Phys. Chem. Lett.* **2016**, *7*, 962−975.

(37) Ho-Wu, R.; Yau, S. H.; Goodson, T., III Linear and Nonlinear Optical Properties of Monolayer-Protected Gold Nanocluster Films. *ACS Nano* **2016**, *10*, 562−572.

(38) Luo, Z.; Yuan, X.; Yu, Y.; Zhang, Q.; Leong, D. T.; Lee, J. Y.; Xie, J. From Aggregation-Induced Emission of Au(I)−Thiolate Complexes to Ultrabright Au(0)@Au(I)−Thiolate Core−Shell Nanoclusters. *J. Am. Chem. Soc.* **2012**, *134*, 16662−16670.

(39) Jiang, X.; Röcker, C.; Hafner, M.; Brandholt, S.; Dörlich, R. M.; Nienhaus, G. U. Endo- and Exocytosis of Zwitterionic Quantum Dot Nanoparticles by Live HeLa Cells. *ACS Nano* **2010**, *4*, 6787−6797.